

Nanoscale tomography in materials science

In materials science, various techniques for three-dimensional reconstruction of microstructures have been applied successfully for decades, such as X-ray tomography and mechanical sectioning. However, in the last decade the family tree of methods has grown significantly. This is partly through advances in instrumentation. The introduction of the focused ion beam microscope and the transformation of transmission electron microscopy into a multipurpose analytical and structural tool have made major impacts. The main driving force for progress is perhaps the advent of nanotechnology with the need to achieve nanometer-scale resolution and the desire to get a real three-dimensional view of the nanoscale world.

Günter Möbus* and Beverley J. Inkson

Department of Engineering Materials, University of Sheffield, Mappin Street, Sheffield S1 3JD, UK

**E-mail: g.moebus@sheffield.ac.uk*

Materials science is a three-dimensional science. Microstructures of bulk materials comprise, for example, anisotropic grains, precipitates, or intergranular phases, while fiber composites are the ultimate anisotropic three-dimensional material. Islands grown on surfaces, dendrites formed from liquids, crack distributions in deformation zones, and the full range of free-standing particles, fibers, and assemblies of these, illustrate further examples. Characterization techniques for materials science in general are, therefore, particularly beneficial if they are able to reveal the richness of microstructure in three dimensions rather than just providing projection views.

Nanostructures differ from micro- and macrostructures by more than just scaling in size. One of the most important aspects is the

surface-to-volume ratio, which increases significantly for nano-objects. This means a sub-10-nm object consists entirely of near-surface structure. Consequently, the importance of characterizing the full three-dimensional structure of these nano-objects similarly increases, as cross sections are even less representative than for bulk materials. Nano-objects exhibit distinct low-dimensionality effects such as quantum confinement. If this confinement applies in all dimensions of space, we speak of a quantum dot or a zero-dimensional structure. Loosely speaking, extreme nanotomography aims at a 'three-dimensional' reconstruction of 'zero-dimensional' objects. In this article, however, we include the entire nanoworld from the 1 nm to the 1 μm length scale, so as to emphasize the breadth and also the industrial relevance of tomography applications in materials science.

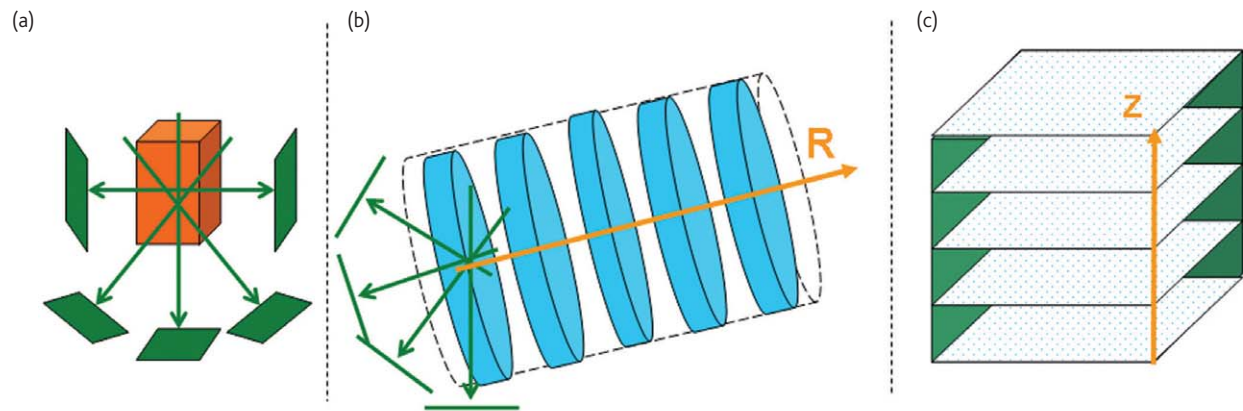


Fig. 1 Principle of electron tomography and reconstruction from sections. (a) Tomographic acquisition: a tilt series of projection images from a three-dimensional volume over a range $\pm 90^\circ$. (b) Tomographic reconstruction: section-wise reconstruction of a cylindrical three-dimensional volume from one-dimensional projections (e.g. columns of the input images from (a)) via two-dimensional cross sections perpendicular to the rotation axis, R. (c) Sectioning: direct three-dimensional reconstruction by interpolation along the normal axis, z, from a stack of section images.

A family tree of tomography methods

Tomography, from its old Greek meaning, is a technique to draw (reconstruct) a section of an object. This refers to inner sections as opposed to surfaces. Since then, tomography has become associated with mapping all inner sections of an object and has therefore become a three-dimensional reconstruction method. The terminology has further developed into:

1. Tomography in a narrow meaning¹, which includes only techniques that collect projection views of an object under various viewing directions (Fig. 1a). In cylindrical geometry, this process is separable into two-dimensional sections perpendicular to the cylindrical (rotation) axis. Reconstruction is achieved slice-by-slice in agreement with the name tomography (Fig. 1b); and
2. Tomography in a wider meaning, which includes all techniques that use sectional views (not only projections) as an intermediate step from which the three-dimensional object is re-assembled (Fig. 1c). This wider definition then covers the field of stereology² and techniques like optical sectioning, confocal microscopy, imaging of mechanically cut parallel sections or iterative etching of materials, and the three-dimensional atom probe, also described in this issue³. This subdivision into projection- and section-based three-dimensional reconstruction is closely related to classification in terms of destructive and nondestructive methods. While tomography in the narrow sense is generally nondestructive as it leaves the specimen unchanged, sectioning can be either, with cutting/etching being destructive while confocal microscopy of transparent objects is nondestructive.

As shown in Fig. 2, some methods provide isotropic resolution and field-of-view in three dimensions, others have particularly high or low resolution in a special z-direction (e.g. normal to a surface), which makes them off-diagonal in an xy versus z resolution diagram.

Three-dimensional reconstruction is all about recovering the missing z-information of an object point in three-dimensional space that is lost

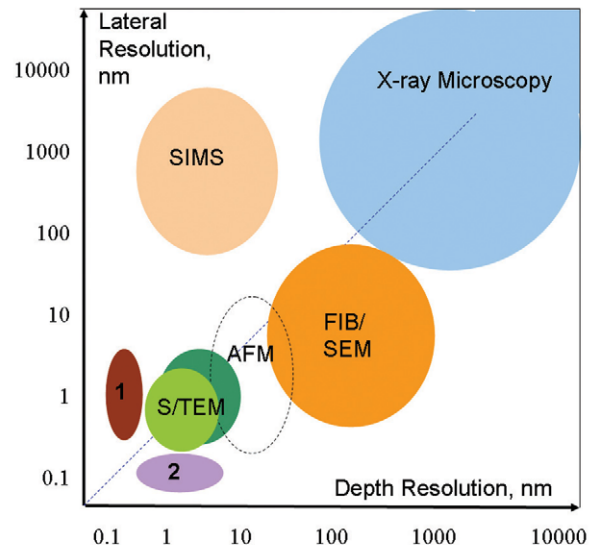


Fig. 2 Length scales of micro-/nanotomography techniques showing lateral versus depth resolution ranges for anisotropic or isotropic techniques. Electron tomography is in green; 1 = atom-probe tomography; 2 = scanning transmission electron microscopy (STEM) focal sectioning; AFM = atomic force microscopy sectioning; SIMS = secondary ion mass spectroscopy; FIB/SEM = focused ion beam/scanning electron microscopy. (Adapted from⁴².)

during projection imaging. This can be obtained by retrieving the z-values of a voxel from multiple xy images, whether as parallax in classic stereology, as amount of point-spread in defocus series (confocal or other microscopy), or as a continuous point trace figure (position versus angle, or a so-called sinogram) in a tomographic tilt series. On the other hand, modern tools for ultrafine cutting and etching of materials while concurrently imaging the fresh surfaces are proving complementary to the other techniques.

This review deals with two methods in greater detail, the first being focused ion beam (FIB) tomography, a destructive sectioning method,

and the second being electron tomography (a nondestructive projection method, tomography in the narrower sense). In a concluding section, we point to some further methods in the field.

Focused ion beam tomography

In order to look inside materials with scientific scrutiny, a block of material must be cut and polished for microscopy observation of thin slices. This was the pioneering concept introduced by Henry Clifton Sorby⁴, who is now seen as the founder of the discipline of 'metallography'. While he studied materials of his time under the light microscope, such as cast iron and geological rock samples, the following century saw the transition to scanning and transmission electron microscopy (SEM and TEM, respectively) to achieve nanoscale lateral resolution. Three-dimensional observations using multiple cuts through the material or repeated etching to free up fresh surfaces were developed, first in biology and then in materials science (see elsewhere for examples^{5–9}).

In order to improve the precision of the cutting or etching steps to match the lateral SEM observation resolution, a new tool needed to be invented: the FIB instrument. Also known as a scanning ion microscope, it can be used both as a nanoscale knife and for ion-beam-induced secondary electron (SE) imaging¹⁰.

The technique

As shown in Fig. 3, FIB tomography is achieved by a series of steps in iteration after preparation of the sample. A flat surface is protected by a sputter-resistant metal coating (e.g. Pt) to achieve sharp edges. An initial trough is milled to a depth Δx , which frees up a sufficient area

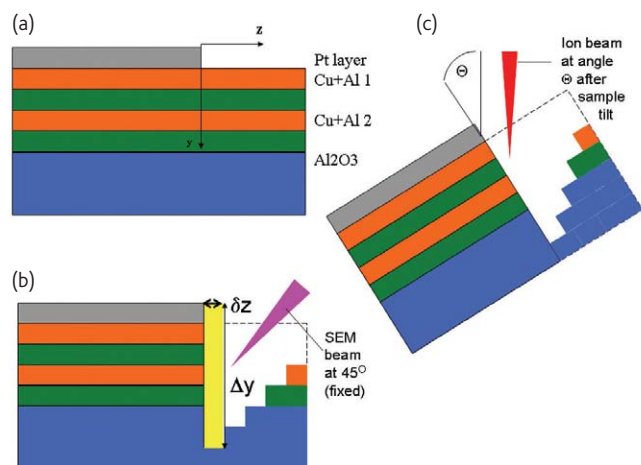


Fig. 3 Principle of FIB tomography using a Cu–Al metallic multilayer ($2 \times \text{Cu} + \text{Al}$) sample as an example (see Fig. 4). (a) Specimen setup with Pt protection layer on the region of interest (invisible in Fig. 4). (b) Iterative three-dimensional sectioning with the freshly milled volume per iteration shown in yellow. Scanning electron microscopy (SEM) imaging in dual-beam instruments. (c) Optional step for single-beam scanning ion microscopy imaging after specimen tilt, Θ . (Adapted from¹⁵.)

of interest ($\Delta x \cdot \Delta y$) of the cross-sectional surface. This becomes the first image of the acquisition, and displays the 'inner microstructure' of the material. Subsequently, imaging and milling of a volume $\delta z \cdot \Delta y \cdot \Delta x$ is alternated, with δz as the increment interval of the sectioning, to acquire an entire three-dimensional stack of fresh surface images. As a final step, three-dimensional interpolation and collation is obtained with specialist software to achieve a continuous three-dimensional volume of material^{11–15}.

The major choice for the technique is whether to use the ion beam for cutting and imaging, or only for cutting. The former has the advantage of generating crisper (higher secondary electron yield) and grain orientation sensitive images (ion channeling), which is beneficial for three-dimensional grain reconstruction¹⁶. However, the need to tilt the sample during every iteration step from its cutting orientation to an imaging angle of, e.g. 45°, is disruptive and increases alignment errors. The cutting and imaging procedures are now mostly shared between ion and electron beams (e.g. fixed at 45°) in a dual-beam instrument. In combination with automated acquisition control software, this configuration has achieved the highest voxel resolution of the technique so far¹⁷ at $\delta z < 50 \text{ nm}$.

While lateral resolution is given by the beam diameter of the field-emission gun scanning electron microscope (FEG-SEM) combined with the SE-emission range, with roughly 1 nm being state-of-the-art, the z-resolution is related to the ion beam diameter and depends strongly on the desirable milling rate (speed), and can achieve 10–100 nm. Ultimately, the z-resolution saturates because the milled surfaces are no longer flat. Reconstruction software to fill three-dimensional volumes from the section images can be easily programmed, with the advantage that a home-grown code can be adapted to possible manual segmentation intervention, specific contrast feature enhancements, or noise suppression. There are also public domain or commercial sector products, such as IMOD¹⁸, Amira¹⁹, or IDL²⁰. The user has to make a decision whether or not to treat the three-dimensional stack as a continuous sample of three-dimensional density values that need to be interpolated. Alternatively, the section images can be reduced after binarization to two-dimensional contours, which are then interpolated in three dimensions by special contour-tracking algorithms.

Applications of FIB tomography

Three-dimensional sectioning using FIB was first targeted at chemical mapping, coupling FIB with secondary ion mass spectrometry (SIMS) for nanocapsules¹³ and semiconductor devices¹⁴. In structural imaging of metals and ceramics, the technique has been adopted to image subsurface deformation microstructure in metallic multilayers on a ceramic substrate^{15,21}, to image the three-dimensional grain shape of polycrystalline metals^{16,22} and to track the three-dimensional distribution of internal cracks formed after scratch loading of a single-crystalline alumina ceramic²³ and after cyclic loading in a dual-phase steel²⁴.

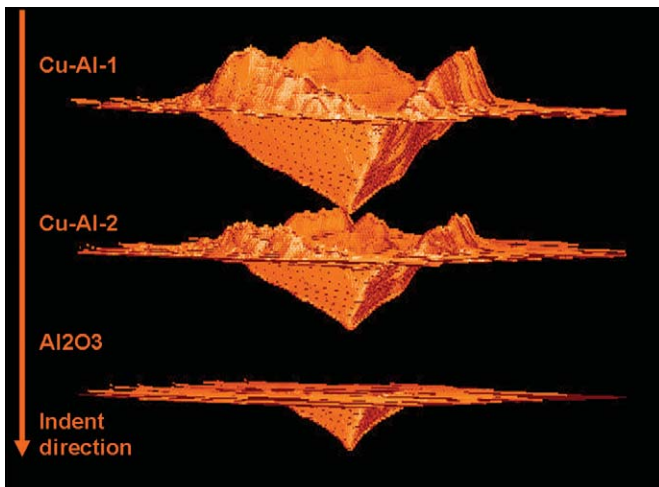


Fig. 4 FIB tomography applied to a Cu–Al metallic multilayer ($2 \times \text{Cu} + \text{Al}$) with a Berkovich indent: (top) outer Cu surface; (center) buried Cu layer; and (bottom) Al_2O_3 substrate surface. $8 \mu\text{m}$ field of view. (Adapted from²¹.)

Fig. 4 shows a Cu–Al multilayer structure on an Al_2O_3 substrate that has been subjected to pyramidal nanoindentation^{15,21}. The top surface shows the highest indentation and pileup amplitude, while the middle buried Cu layer shows reduced deformation. The substrate surface shows no pileup and only a small residual plastic indent. The latter two surfaces are located inside the material and would be inaccessible to AFM.

A second example is in visualizing nano- and microstructures of particle granularity in cement (Fig. 5)^{25,26}. After compaction, the particle morphology and statistical distribution is evaluated from the three-dimensional FIB stack. Contrast enhancement by filling pores with high-Z metal has been employed successfully in this application. Further areas where FIB tomography has proven highly promising include nanoporous materials¹⁷, superalloys²², and semiconductor nanostructures and devices^{27,28}.

SE imaging as the major source of image acquisition has been recently extended to include energy-dispersive X-ray (EDX) chemical maps^{29,30}, which allows chemical identification of phases along with element-specific three-dimensional reconstruction. The first steps in electron backscatter diffraction (EBSD)-mapping combined with serial sectioning for grain orientation crystallography have also been made³¹.

Electron tomography

The equivalence, in principle, of using electrons and photons to generate projection data in a transmission geometry through three-dimensional materials led to the introduction of transmission electron microscopy (TEM) tomography^{1,32,33} not long after X-ray tomography was introduced as a concept³⁴. However, because of the much stronger interaction of electrons with matter, the linearity of projection (with intensity being proportional to the thickness times density) is quite limited in TEM. For decades, therefore, electron tomography remained

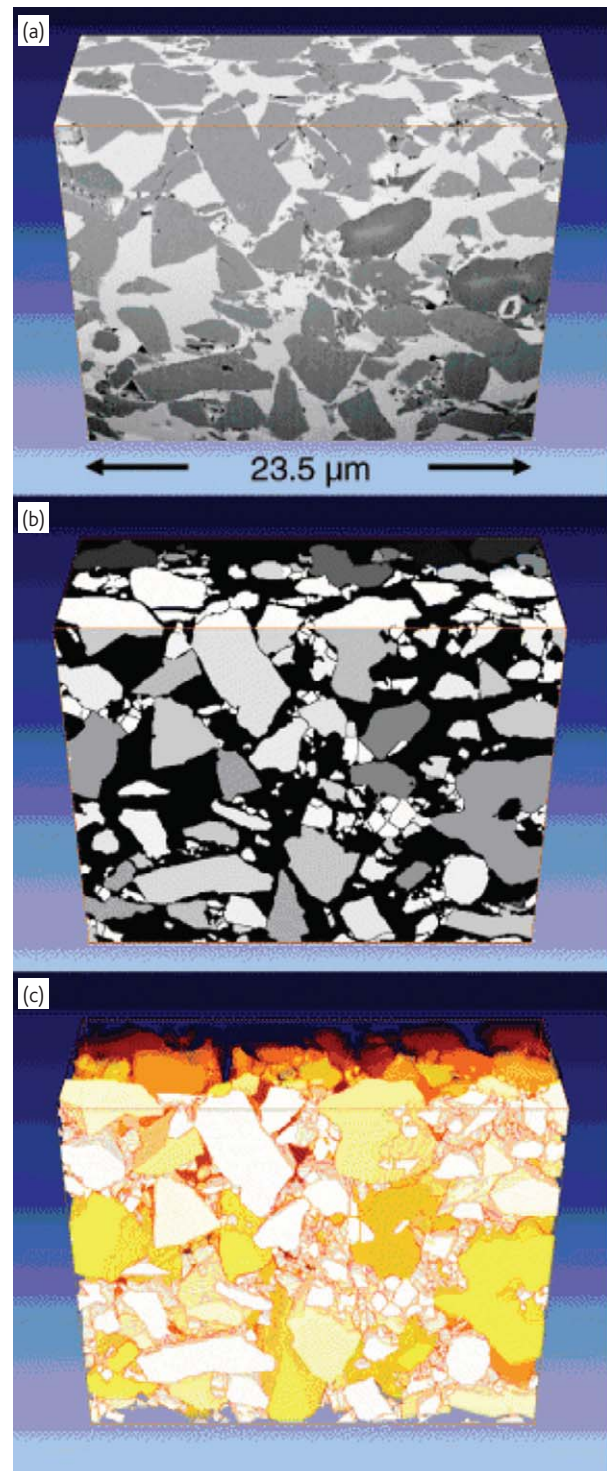


Fig. 5 FIB tomography applied to a cement particulate system. Grains from an ordinary Portland cement (OPC) sample appear dark and are impregnated with a metal alloy (bright) after compacting the dry powder in order to improve image contrast and assist segmentation. (a) Raw data after alignment and preprocessing; (b) after segmentation; and (c) semitransparent visualization, where each particle is labeled with a specific color value. Cube size: $23.5 \times 19.2 \times 9.5 \mu\text{m}$. Voxel resolution: $30 \times 38 \times 60 \text{ nm}$. Number of particles in box: 1404. (Reprinted with permission from²⁵. © 2006 Blackwells Publishing.)

a niche technique for applications with carbon or carbohydrate-based amorphous materials typical of the biomedical field (viruses, cell organelles, etc.). X-ray tomography meanwhile moved faster into materials science, see for example^{35,36}. The main problems that arise in wider materials science are the atomic-number-dependent absorption limit for maximum useful thickness³⁷ and the high coherence of electrons leading to interference patterns in crystalline materials through Bragg scattering, which mostly destroys tomographic contrast.

Biomedical electron tomography relies on one of two projection mechanisms for two regimes of thickness¹. For ultrathin samples, the weak-phase object linear approximation holds. For objects thicker than a few nanometers, a Beer law exponential absorption contrast in bright-field TEM starts to dominate, which can be easily linearized. This biomedical bright-field electron tomography was later easily copied for carbon-only materials (e.g. carbon-black nanoparticles³⁸ or polymeric materials³⁹), and a first successful inorganic application has been achieved for mesoporous silicate catalyst supports⁴⁰.

For a completely general application to the entire field of inorganic materials science, especially inorganic nanotechnology, a new mode of electron tomography was needed that eliminated coherent scattering artifacts. Energy-filtered (EF)-TEM, or spectroscopic imaging^{41,42}, and high-angle annular dark-field (HAADF) scanning transmission electron microscopy (STEM)^{43–45} have been introduced and demonstrated to achieve this aim. A rapid advance of the field has since been observed worldwide, which was first reviewed in this journal three years ago⁴⁶.

Electron tomography modes

Almost every imaging mode that produces TEM images or STEM maps has been tested for applicability in materials tomography in the last five years. We classify these approaches into three groups^{47,48}.

1. Shape-sensitive methods. These include all modes that reliably reproduce the contour of an object, with bright-field TEM (after contrast inversion and binarization) being the simplest, and also including conventional dark-field techniques and STEM imaging, as mentioned below.
2. Density-sensitive methods. Since neutrons do not contribute to electron scattering, density always refers to atomic-number density rather than mass density. An average atomic number per voxel is reconstructed, which gives these techniques a certain chemical sensitivity with potential for phase mapping. In a future scenario, when TEM resolution and alignment improvements allow the reduction of voxel size to atomic diameters, this method will convert to a full elemental mapping method as below. Suitable modes include HAADF-STEM and its equivalent C-TEM Z-contrast modes.
3. Elemental-mapping methods. Using spectroscopic imaging modes, which allow tuning of a spectrometer to pass signals from one chemical element only, we can achieve spectroscopic electron

tomography. If applied to entire spectra or consecutively to various energy windows, this technique returns a four-dimensional data volume with $(x,y,z,\delta E)$ as a four-dimensional voxel where δE is the spectroscopic energy. Each tomogram for energy δE contains the density of one element per voxel only, suppressing the existence of other elements. Spectroscopic electron tomography has been demonstrated using both EF-TEM imaging⁴¹ and EDX mapping⁴². The main advantage of EDX tomography is that it has the highest thickness limit of all electron tomography modes and allows the simultaneous acquisition of all spectroscopic energies (elements). The need for special holders that do not shade the X-ray paths to the detector⁴², prolonged X-ray acquisition times, and fluorescence scattering artifacts (anisotropic detector geometry) are drawbacks.

Discussions of bright-field TEM versus high- and low-angle ADF-STEM can be found elsewhere^{49,50}. A comparison of all three groups of methods applied to one materials example is shown in Fig. 6⁴⁸, where bright-field TEM, EF-TEM, and ADF-STEM tomographies are used to reconstruct CeO₂ nanoparticles. The success of the bright-field reconstruction, in spite of strong Bragg scattering artifacts, is mostly because of the convexity and constant density of the particles⁴⁸. The EF-TEM reconstruction is artifact-free in its projection images and benefits from simultaneous acquisition together with a BF tilt series. It is performed here with a single-energy window including the Ce-N-edge at around 130 eV because there are no chemical mapping needs. The ADF-STEM reconstruction, obtained on a separate but equivalent particle, is also artifact-free. A parallel acquisition of

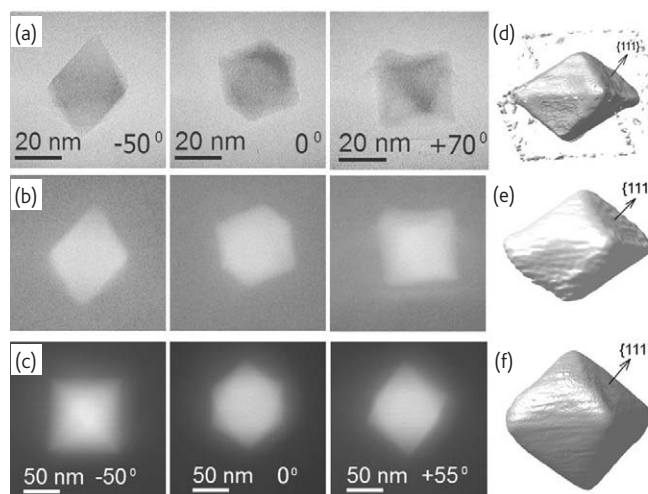


Fig. 6 Electron tomography of individual CeO₂ nanoparticles. Examples of projection images from a tilt series taken in (a) bright-field TEM, (b) EF-TEM, (c) and ADF-STEM. The first two tilt series are from an identical particle acquired pair-wise, while (c) is from a different particle. Isosurface views of reconstructed particles, (d), (e), and (f), as obtained from the full tilt series behind (a), (b), and (c), respectively. Untruncated octahedral morphology enclosed by {111} crystallographic planes as concluded from accompanying electron diffraction experiments. (Reprinted with permission from⁴⁸. © 2007 Institute of Physics Publishing.)

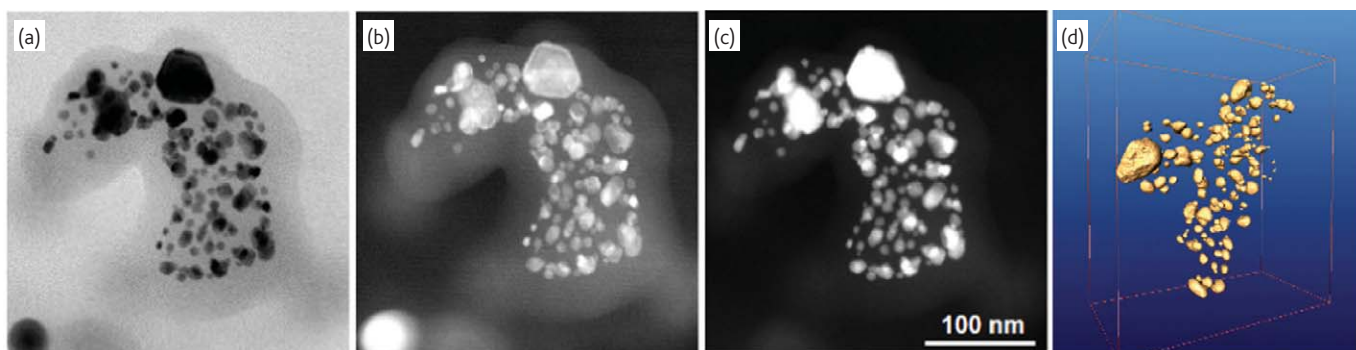


Fig. 7 Pt catalyst nanoparticles embedded in a carbon matrix. (a) Bright-field TEM, (b) ADF-STEM, and (c) HAADF-STEM images with (d) a three-dimensional reconstruction from a tilt series of (c) to highlight the metal particles while the carbon matrix appears invisible. (Reprinted with permission from⁵⁰. © 2006 Institute of Physics Publishing.)

a bright-field STEM tilt series would be equally possible on some microscopes.

An important point is the angular range of the tilt series. The closer the full tilt range of $\pm 90^\circ$ is approached, the fewer anisotropy artifacts will occur. It has been necessary to design novel specimen holders^{44,51} to fit into typical narrow pole-piece gaps for modern high-resolution TEMs in order to increase the tilt limit from the $\pm 15\text{--}40^\circ$ that was previously typical to over $\pm 60\text{--}80^\circ$. Reconstruction of the data can again be achieved with a choice of commercial, public domain¹⁸, or home-grown codes, with weighted backprojection¹ being the most widespread technique. Further coverage of data-processing techniques can be found elsewhere in this issue⁵².

Applications of electron tomography in materials science

Examples of materials science areas that are particularly suitable for electron tomography have been identified by a growing number of research labs. They include the following fields.

Catalysis

Catalyst and petrol industries, or pollution-sensitive industries in general, are keen to optimize catalytic performance. Knowledge of the detailed three-dimensional pore structure of supports, as well as the distribution and preferred adhesion sites of active particles, provides important feedback for catalyst design and fabrication. Heavy metal catalyst particles on low-Z or porous substrates are a highly promising target for tomographic reconstruction. Fig. 7 shows Pt nanoparticles in carbon using HAADF-STEM⁵⁰, and a similar example is found elsewhere⁵³. Fig. 8 shows Au particles in a mesoporous silicate by bright-field TEM⁵⁴.

Glasses

Nanoparticles in glasses are one example from the large application field of glass-ceramic composites that are highly suitable for electron tomography. They also benefit from the usually low atomic number of the glass matrix, which can be separated from heavier precipitates^{55,56}.

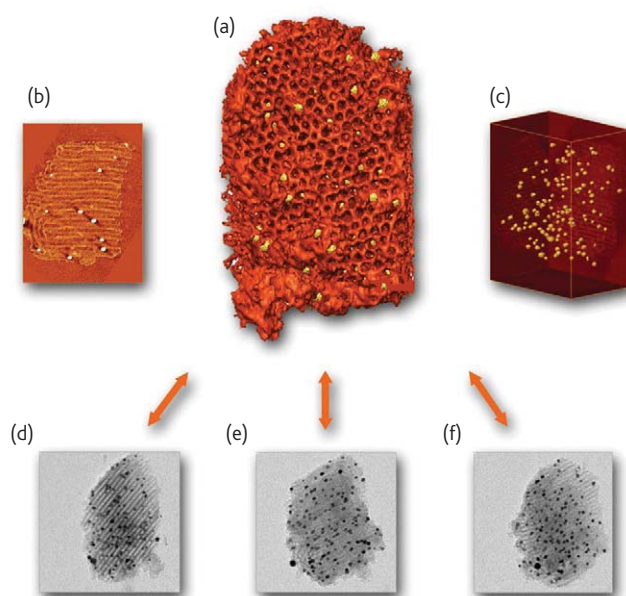


Fig. 8 Au catalyst nanoparticles inside a SBA-15 mesoporous support. (a) Surface-rendered view of the three-dimensional reconstruction. Volume size $\sim 256 \times 256 \times 166$ nm. (b) Virtual cross section cut from (a). (c) Surface rendering of Au particles only. (d)–(f) Three examples of bright-field TEM projection images from a tilt series of 151 micrographs from -55° to $+55^\circ$ used to calculate the reconstruction in (a). (Reprinted with permission from⁵⁴. © 2004 Elsevier.)

Metals and alloys

Oxide dispersion ceramic nanoparticles in an intermetallic FeAl matrix have been reconstructed⁴², as have Cr precipitates in grain boundaries in steel⁴⁴. Exploration of strengthening mechanisms by deliberate particle inclusion, as well as weakening mechanisms by grain boundary embrittlement, will benefit from this type of chemical- and phase-sensitive tomography.

Electronic devices

The highly complex three-dimensional integration of transistor and interconnect nanostructures in modern semiconductor device

fabrication lines is a world away from the early days of planar wafer dopant patterning. Not surprisingly, the semiconductor industry has reported the first in-house industrial application of nanoscale inorganic electron tomography using ADF-STEM⁵⁷, with further semiconductor applications found elsewhere⁵⁸.

Nanoparticles and nanowires

Knowledge of the surface morphology and crystallographic facets of nanoparticles helps in tuning their functional properties and gives feedback to mass-production process lines. For multiphase particles or core-shell objects, tomography is essential to reveal three-dimensional chemical maps. Examples of applications include reconstructions of magnetite crystals of biological origin^{44,49}. Pd⁵⁹ and Cu⁶⁰ are just two examples of several tomography research projects on metal nanoparticles, while ceramic particles (CeO₂) have also been investigated⁴⁸. Si nanowires are an example of one-dimensional nano-objects⁶¹. The shape and core-shell structure of W nanowires have also been reported⁶².

Dislocations

Distribution mapping of dislocations by dark-field TEM is perhaps the oldest TEM application where the radical need for three-dimensional reconstruction was realized. Traditionally solved by stereology from a pair of viewing directions, a recent demonstration⁶³ using a full tilt series with tomographic reconstruction shows benefits as the backprojection resolves the need for semimanual dislocation line positional tracking.

Biomaterials

Biomaterials provide a bridge between the new world of materials electron tomography and the older field of tomography of cell structures. Biomaterials often benefit from the same low atomic number and mostly amorphous structures typical of biomedical

tomography, and therefore have great potential. Fig. 9 shows an example from bone-mineralization research, in which collagen-fibrils are reconstructed in three dimensions⁶⁴.

Further nanoscale sectioning tomographies

This review of nanoscale three-dimensional reconstruction methods would be incomplete without three recently introduced complementary methods. These all belong to the serial-sectioning and anisotropic part of the family tree of tomographic methods (off-diagonal in Fig. 2), with the first two being destructive. The three-dimensional atom probe⁶⁵ would also feature prominently here, but is covered elsewhere in this issue³.

Three-dimensional nanoSIMS and related approaches are an evolution from standard SIMS with a reduced beam diameter to provide higher spatial resolution^{66,67}. The technique still lags behind FIB tomography in terms of lateral resolution, however depth resolution can be excellent, and its main advantage is three-dimensional chemical imaging⁶⁸. One drawback is SIMS-specific artifacts, such as layer-mixing and unequal sputtering rates for various elements. Related ablation techniques exist, such as laser-induced breakdown spectroscopy (LIBS), which also have great potential for three-dimensional mapping⁶⁹.

AFM sectioning⁷⁰ is the nanoscale extension of various etching-based sectioning techniques on the micronscale (e.g. using light microscopy). The method has been demonstrated using plasma etching of 7.5 nm thick layers of a styrene-*block*-butadiene-*block*-styrene (SBS) sample⁷⁰ and liquid cell etching for a bone sample⁷¹. Phase-dependent etching speeds and curvature of the surfaces have been identified as limitations and correction procedures have been proposed⁷¹. The latest variation of the topic is an AFM-ultramicrotome combination for iterative sectioning⁷².

Sectioning STEM using low depth of focus electron illumination is at an early stage of development. Computer simulations have demonstrated the possibility of focusing electron beams into materials below their surface. This has opened the new possibility of three-dimensional reconstruction by imaging a STEM condenser focal series with minimized depth-of-focus^{73–76}. Unlike high-resolution STEM, the condenser aperture needs to be opened to a maximally tolerable value, or even better C_s-corrected condensers should be used. The necessary extraction of the focused information can be done in various ways, such as the use of a pinhole-equivalent point-detector (for bright-field STEM), and is aptly named 'confocal STEM' as it is equivalent to an optical microscope⁷⁷. First experiments on sectioning in STEM have been conducted to image single atoms^{78,79} with an aberration-corrected condenser lens. Application to nanoparticles a few nanometers in size seems to be within reach even without a C_s-corrector⁸⁰. Fourier-space filters can help extract the in-focus information without a confocal setup while preserving the advantage of HAADF imaging⁸⁰. A double C_s-corrected microscope seems to be the

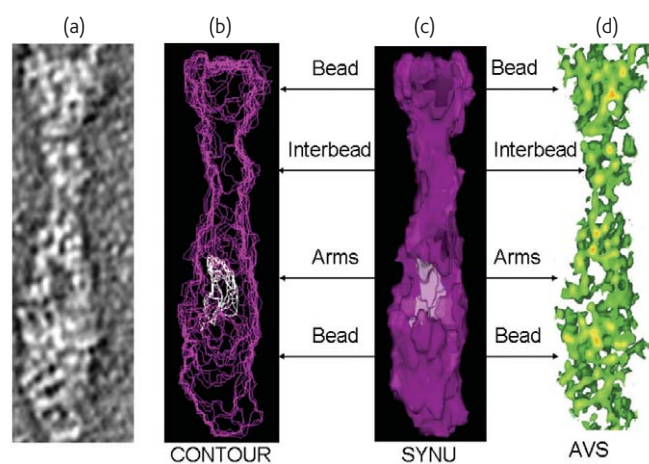


Fig. 9 Electron tomography of biomaterials. Three-dimensional reconstruction of fibrillin microfibrils. Field-of-view of 56 nm, corresponding to one repeat unit of the structure. (a) Experimental image from a tilt series and (b)–(d) use of three different software packages to display the three-dimensional reconstruction. (Reprinted with permission from⁶⁴. © 2002 Elsevier.)

ultimate instrument for this application^{74,76} and a confocal STEM setup with two C_s-correctors has been experimentally realized⁸¹.

Conclusions

Nanoscale tomography is a vibrant and multifaceted research field that is currently experiencing rapid growth in materials science. The driving forces for progress in methodology have been, and will continue to be, the quest for higher resolution. This is expected to continue until atomic-level resolution is reached. Furthermore, the benefit of adding further dimensions beyond the three spatial dimensions (such as time

or spectroscopic energy) is proving promising. Ultimately, full process control in materials fabrication and materials in-service monitoring requires a characterization technique with a chemically and structurally sensitive 'eye' and three-dimensional vision. Speed, accuracy, robustness against artifacts, and adaptation to a particular materials problem will be the criteria against which a choice is made from the extended family of tomographic methods. **mt**

Acknowledgments

We are thankful to Xiaojing Xu, Zineb Saghi, and Ralph Gay for helpful contributions.

REFERENCES

- Frank, J., *Electron Tomography: Three-dimensional Imaging with the Transmission Electron Microscope*, 2nd ed., Plenum Press, New York, (2007)
- Russ, J. C., and Dehoff, R. T., *Practical Stereology*, Plenum Press, New York, (2000)
- Cerezo, A., et al., *Materials Today* (2007) **10** (12), 36
- Sorby, H., *J. Iron Steel Inst.* (1887) **1**, 255
- McDowall, A. W., et al., *J. Microsc.* (1983) **131**, 1
- Bron, C., et al., *Proc. SPIE* (1990) **1245**, 61
- Li, M., et al., *Mater. Characterization* (1996) **41**, 81
- Martinez, S. J., and Pinoli, J.-C., *J. Comput.-Assisted Microsc.* (1996) **8**, 131
- Alkemper, J., and Voorhees, P. W., *J. Microsc.* (2001) **201**, 388
- Orloff, J., et al., *High resolution Focused Ion Beams: FIB and its Applications*, Kluwer, New York, (2003)
- Uchic, M. D., et al., *MRS Bull.* (2007) **32**, 408
- Sakamoto, T., et al., *Jpn. J. Appl. Phys., Part 1* (1998) **37** (4 suppl. A), 2051
- Tomiyasu, B., et al., *Nucl. Instrum. Methods Phys. Res., Sect. B* (1998) **136-138**, 1028
- Dunn, D. N., and Hull, R., *Appl. Phys. Lett.* (1999) **75**, 3414
- Inkson, B. J., et al., *J. Microsc.* (2001) **201**, 256
- Inkson, B. J., et al., *Scripta Mater.* (2001) **45**, 753
- Holzer, L., et al., *J. Microsc.* (2004) **216**, 84
- Kremer, J. R., et al., *J. Struct. Biol.* (1996) **116**, 71
- Amira, Mercury computer systems, Inc., USA, www.tgs.com
- IDL, Interactive Data Language, ITT Corp., USA, www.itervis.com/idl
- Steer, T. J., et al., *Thin Solid Films* (2002) **413**, 147
- Uchic, M. D., et al., *Scripta Mater.* (2006) **55**, 23
- Wu, H. Z., et al., *Acta Mater.* (2003) **51**, 149
- Motoyashiki, Y., et al., *Fatigue Fracture Eng. Mater. Struct.* (2007) **30**, 556
- Holzer, L., et al., *J. Am. Ceram. Soc.* (2006) **89**, 2577
- Münch, B., et al., *J. Am. Ceram. Soc.* (2006) **89**, 2586
- Inkson, B. J., et al., *Inst. Phys. Conf. Ser.* (2003) **180**, 611
- Yeoh, T. S., et al., *Mater. Res. Soc. Symp. Proc.* (2006) **908E**, 0908-0005-11.1
- Kotula, P. G., et al., *Microsc. Microanal.* (2006) **12**, 36
- Schaffer, M., et al., *Ultramicroscopy* (2007) **107**, 587
- Groeber, M. A., et al., *Mater. Characterization* (2006) **57**, 259
- de Rosier, D. J., and Klug, A., *Nature* (1968) **217**, 130
- Hoppe, W., et al., *Naturwissenschaften* (1968) **55**, 333
- Cormack, A. M., *J. Appl. Phys.* (1963) **34**, 2722
- Haddad, W. S., et al., *Science* (1994) **266**, 1213
- Baruchel, J., et al., *Scripta Mater.* (2006) **55**, 41
- Levine, Z. H., *Proc. SPIE* (2005) **5674**, 1
- Hunt, E. M., and Herd, C. R., *Microsc. Microanal.* (2001) **7** (suppl. 2), 82
- Spontak, R. J., et al., *Macromolecules* (1996) **29**, 2850
- Koster, A. J., et al., *J. Phys. Chem. B* (2000) **104**, 9368
- Möbus, G., and Inkson, B. J., *Appl. Phys. Lett.* (2001) **79**, 1369
- Möbus, G., et al., *Ultramicroscopy* (2003) **96**, 433
- Midgley, P. A., et al., *Chem. Commun.* (2001), 907
- Midgley, P. A., and Weyland, M., *Ultramicroscopy* (2003) **96**, 413
- Koguchi, M., et al., *J. Electron Microsc.* (2001) **50**, 235
- Weyland, M., and Midgley, P. A., *Materials Today* (2004) **7** (12), 32
- Möbus, G., and Inkson, B. J., *Microsc. Microanal.* (2003) **9** (suppl. 2), 176
- Xu, X., et al., *Nanotechnology* (2007) **18**, 225501
- Friedrich, H., et al., *Ultramicroscopy* (2005) **106**, 18
- Cervera Gontard, L., et al., *J. Phys., Conf. Ser.* (2006) **26**, 203
- Möbus, G., et al., *Microsc. Microanal.* (2004) **10** (suppl. 2), 1196
- Sakellariou, A., et al., *Materials Today* (2007) **10** (12), 44
- Wikander, K., et al., *J. Colloid Interface Sci.* (2007) **305**, 204
- Ziese, U., and Koster, A. J., *Appl. Catal. A* (2004) **260**, 71
- Xu, X. J., et al., *Mater. Res. Soc. Symp. Proc.* (2007) **928E**, 0982-KK02-04
- Yang, G., et al., *Mater. Res. Soc. Symp. Proc.* (2007) **985**, 0985-NN06-01
- Stegmann, H., et al., *Microelectron. Eng.* (2002) **65**, 171
- Kübel, C., et al., *Microsc. Microanal.* (2005) **11**, 378
- Park, J.-B., et al., *Appl. Phys. Lett.* (2007) **90**, 093111
- Oikawa, T., et al., *Microsc. Microanal.* (2006), **12** (suppl. 2), 616
- Arbiol, J., et al., *Mater. Res. Soc. Symp. Proc.* (2004) **818**, M.4.5
- Xu, X., et al., *J. Phys. Conf. Ser.* (2007) **61**, 810
- Barnard, J. S., et al., *J. Phys. Conf. Ser.* (2006) **26**, 247
- Baldock, C., et al., *J. Struct. Biol.* (2002) **138**, 130
- Miller, M. K., *J. Microsc.* (1997) **186**, 1
- McPhail, D. S., *Appl. Secondary Ion Mass Spectrom. Mater. Sci.* (2006) **41**, 873
- Zaitsev, V. S., et al., *Mater. Res. Soc. Symp. Proc.* (2000) **661**, K.K.6.2
- Hutter, H., et al., *Fresenius J. Anal. Chem.* (1993) **346**, 66
- Nicolas, G., et al., *J. Anal. Atomic Spectrom.* (2007), doi: 10.1039/b704682k
- Magerle, R., *Phys. Rev. Lett.* (2000) **85**, 2749
- Dietz, C., et al., *Rev. Sci. Instrum.* (2007) **78**, 053703
- Efimov, A. E., et al., *J. Microsc.* (2007) **226**, 207
- Möbus, G., *Proc. EUREM 12*, CSEM, Brno, (2000) **1**, 385
- Möbus, G., et al., *Inst. Phys. Conf. Ser.* (2001) **168**, 27
- Möbus, G., and Nufer, S., *Inst. Phys. Conf. Ser.* (2001) **168**, 151
- Möbus, G., and Nufer, S., *Ultramicroscopy* (2003) **96**, 285
- Einspahr, J. J., and Voyles, P. M., *Ultramicroscopy* (2006) **106**, 1041
- Lupini, A. R., et al., *Inst. Phys. Conf. Ser.* (2003) **180**, 523
- Van Benthem, K., et al., *Appl. Phys. Lett.* (2005) **87**, 034104
- Möbus, G., et al., *Proc. 16th Int. Microsc. Congr.* (2006) **2**, 949
- Nellist, P. D., et al., *Appl. Phys. Lett.* (2006) **89**, 124105